Biosensors and Bioelectronics 144 (2019) 111560

Contents lists available at ScienceDirect

Biosensors and Bioelectronics

journal homepage: www.elsevier.com/locate/bios

Target-inspired Pb^{2+}-dependent DNAzyme for ultrasensitive electrochemical sensor based on MoS_2-AuPt nanocomposites and hemin/G-quadruplex DNAzyme as signal amplifier

Renyue Ji[1], Wuceng Niu[1], Shuai Chen, Wei Xu, Xingduo Ji, Lingyue Yuan, Hangyu Zhao, Minghao Geng, Jingfu Qiu[*,1], Chaorui Li[**,1]

School of Public Health and Management, Chongqing Medical University, Box 197#, No.1,Yi Xue Yuan Road, Yuzhong District, Chongqing, 400016, China

ARTICLE INFO

Keywords:
Electrochemical DNAzyme sensor
Pb^{2+}-dependent DNAzyme
MoS_2–AuPt nanocomposites
Hemin/G-quadruplex
rGO-SnO_2

ABSTRACT

In this work, a novel Pb^{2+} electrochemical DNAzyme sensor was developed for ultrasensitive detection of lead ions (Pb^{2+}) in water environment by coupling with the MoS_2–AuPt nanomaterials and hemin/G-quadruplex DNAzyme, which acting as the electrocatalytic signal tag. Streptavidin (SA) modified tin dioxide-functionalized reduced graphene oxide (rGO-SnO_2) /gold nanoparticles (AuNPs) served as a sensor platform for enhancing conductivity and immobilizing more Pb^{2+}-specific DNAzyme. In the presence of Pb^{2+}, the Pb^{2+}-dependent DNAzyme specifically reacted with Pb^{2+}, cleaving the substrate strand (SS) into two free fragment and releasing the biotin-modified enzyme strand (Bio-ES) on the electrode. Connecting MoS_2–AuPt nanocomposites labeled with G-rich DNA (G-DNA) strand and exposure of Bio-ES through the Helper DNA, as well as adding hemin to form a hemin/G-quadruplex, the biosensor achieved signal amplification. Chronoamperometry was used to record the current signal, which was primarily derived from the cocatalysis reduction of H_2O_2 by MoS_2–AuPt nanocomposites and the hemin/G-quadruplex. Under optimal conditions, the designed biosensor exhibited sensitive detection of Pb^{2+} from 0.1 pg mL^{-1} to 1000 ng mL^{-1}, with a lower detection limit of 38 fg mL^{-1} (based on 3σ). This proposed biosensor is ultrasensitive and specific, representing a potential application for the detection of Pb^{2+} in a water environment.

1. Introduction

The lead ion (Pb^{2+}) is a widespread and highly toxic heavy metal pollutant in the water environment (Li et al., 2014b). Because of its bioaccumulative and nonbiodegradable nature, lead ions can cause neurological, reproductive, cardiovascular and developmental disorders, even at low concentrations (Dong et al., 2015; Huang et al., 2018; Liu et al., 2016; Wang et al., 2018; Xu et al., 2018a). Considering the detrimental effects of lead ions, developing sensitive and selective methods for Pb^{2+} detection are of great significance. Routine analytical techniques for Pb^{2+} detection include atomic absorption spectroscopy (AAS) (Behbahani et al., 2015), atomic emission spectrometry (AES) (Yu et al., 2017), inductively coupled plasma mass spectrometry (ICP-MS) (Shamsipur et al., 2017), and anodic stripping voltammetry (ASV) (Sun et al., 2017). Although these methods are sensitive and reliable for Pb^{2+} detection, they typically require complicated operational procedures and sophisticated equipment, limiting their practical application. To overcome these limitations, we utilized electrochemical biosensors, which provide a promising platform for Pb^{2+} detection due to their advantages of high sensitivity, simple operation, cost-effectiveness and rapid detection (Bingqian et al., 2012; Gang et al., 2017; Murali et al., 2014; Zhang et al., 2015a).

DNAzyme, a method for in vitro selection of DNA sequences, is a DNA-based enzyme with enzymatic catalytic activities, and have been widely applied for the highly sensitive detection of metal ions (Feng et al., 2015; Huang et al., 2019; Wang et al., 2018; Xue et al., 2016; Yang et al., 2016; Yin et al., 2017; Zhao et al., 2019; Zou et al., 2017). One type of DNAzyme, namely, 8–17 DNAzyme is a double-stranded DNA and is a DNA metalloenzyme catalyzing RNA transesterification in the presence of divalent metal ions. It is composed of an enzyme strand (ES) and a substrate strand (SS), and the SS contains a single ribonucleobase (RNA) linkage (such as 'rA') that serves as the specific cleavage

* Corresponding author.
** Corresponding author.
E-mail addresses: jfqiu@126.com (J. Qiu), crli@cqmu.edu.cn (C. Li).
[1] Renyue Ji and Wuceng Niu contributed equally to this work.

https://doi.org/10.1016/j.bios.2019.111560
Received 27 May 2019; Received in revised form 30 July 2019; Accepted 31 July 2019
Available online 03 August 2019
0956-5663/

site (Bleul et al., 2016; Gang et al., 2017). In the presence of Pb^{2+}, the SS can be recognized and cleaved into two fragments at the 'rA' site, thus leaving the ES exposed to match with a signal tag and further detect target Pb^{2+} as an amplification strategy (Guo et al., 2012; Wang et al., 2017; Zhou et al., 2016). Therefore, the development of the assay combine with Pb^{2+}-dependent DNAzyme-based biosensor for the sensitive detection of Pb^{2+} is highly desirable.

In order to improve the sensitivity and stability of electrochemical biosensor, amount of efforts have been devoted to immobilization of the 8–17 DNAzyme on the electrode. Recently, two-dimensional (2D) nanolayer materials have attracted widespread attention. One of the 2D nanolayer materials is tin dioxide-functionalized reduced graphene oxide (rGO-SnO_2), which is considered a desirable nanomaterial used as nanocarriers because of its large specific surface area and high mobility conducting electrons (Li et al., 2014a). In this work, we prepared the (3-Aminopropyl) triethoxysilane (APTES)-modified rGO-SnO_2 (APTES-rGO-SnO_2) containing a large number of the amino group, which could be an ideal template for loading gold nanoparticles (AuNPs) to further enhance its performance. In addition, APTES–rGO–SnO_2/AuNPs can combine with streptavidin (SA) via the amino-Au affinity to increase the biotin-modified ES (Bio-ES) of 8–17 DNAzyme loading onto the surface of the electrochemical biosensor through the biotin-streptavidin system, which has high specificity and an extraordinarily high affinity for biotin. Thus, the APTES-rGO-SnO_2 has shown great promise as electrode substrate materials.

To achieve signal amplification of the electrochemical biosensor, many enhancers like metal catalyst (Zhou et al., 2016), peroxidase (Wang et al., 2018a), thionine (Wang et al., 2016), and methylene blue (Liu et al., 2018) were applied in biosensor. In the metal catalyst, contributing to catalytic activity and chemical selectivity, bimetallic AuPt nanoparticles provide variations in chemical and physical properties, compared with single Pt nanoparticles and single Au nanoparticles (Cui et al., 2015; Wang et al., 2014; Zhuang et al., 2016). Additionally, MoS_2 nanosheets, as 2D nanolayer materials, are a type of transition metal sulfide constructed by stacking covalently bound S–Mo–S through weak Van der Waals interactions, which have unique nanosheet structural features and large specific surface area (Vishnu and Badhulika, 2019). Specially, MoS_2 nanosheets can easily load a large number of metal nanoparticles as a sensing platform to synthesize nanocomposites, which could further enhance the electrochemical signal response and show excellent properties (Ji et al., 2018). Therefore, AuPt NPs were employed in combination with MoS_2 nanosheets to synthesize MoS_2–AuPt nanocomposites which can further enhance the surface area, facilitate electron transfer and improve the electrochemical conductivity (Ji et al., 2018; Xu et al., 2018b). In this regard, MoS_2–AuPt nanocomposites are a promising candidate for fabrication of biosensors to produce and amplify the electrochemical signal by the catalysis of hydrogen peroxide (H_2O_2). Meanwhile, through the Au–NH_2 bonds and the Pt–NH_2 bonds, MoS_2–AuPt nanocomposites combined with G-rich DNA (G-DNA) that can match with the Helper DNA, which was applied as the signal tag in this signal amplification strategy for the Pb^{2+} detection. Additionally, hemin/G-quadruplex DNAzyme is a known horseradish peroxidase mimicking DNAzyme and is formed by binding a G-DNA strand with a hemin molecule (Gao et al., 2017; Yang et al., 2015). To further enhance the signal amplification, It was used with MoS_2–AuPt nanocomposites to co-catalyze H_2O_2-mediated oxidation reactions to produce signal so that it can be conveniently used in electrochemical sensors as a signal amplification strategy (Chen et al., 2017b; He et al., 2013; Zhang et al., 2015b).

Herein, we report a highly sensitive platform for Pb^{2+} detection based on the cocatalysis of MoS_2–AuPt nanocomposites and hemin/G-quadruplex-based DNAzyme. First, Pb^{2+}-specific DNAzyme was immobilized on a SA-functionalized APTES-rGO-SnO_2/AuNPs platform which can increase the sensitivity of the biosensor. In the presence of Pb^{2+}, Pb^{2+}-dependent DNAzyme was specifically identified and cleaved by Pb^{2+}, resulting in exposure of Bio-ES on the biosensor. Next, Helper DNA, as intermediate bridges, connected MoS_2–AuPt nanoparticles labeled with G-DNA strands, exposing Bio-ES through the hybridization reaction. Subsequently, the G-DNA strand combined with hemin to form a hemin/G-quadruplex DNAzyme structure for an electrochemical catalysis signal. The application of Pb^{2+}-dependent DNAzyme improved the selectivity of the electrochemical biosensor, whilst utilization of MoS_2–AuPt nanocomposites and hemin/G-quadruplex-based DNAzyme co-catalyze H_2O_2 to amplify the electrochemical signal and further enhanced the sensitivity. This proposed electrochemical biosensor displays high specificity, good stability, and a low detection limit, suggesting its great potential for applications in Pb^{2+} quantitative determination.

2. Experimental methods

2.1. Reagents and chemicals

rGO-SnO_2 was purchased from Nanjing XFNANO Materials TECH Co., Ltd. (China). MoS_2 nanosheets (Diameter 20–500 nm) were obtained from Nanjing JCNANO Technology Co., Ltd. (Nanjing, China, www.jcnano.com). Gold chloride ($HAuCl_4{\cdot}4H_2O$), chloroplatinic acid ($H_2PtCl_6{\cdot}6H_2O$), SA, hemin, bovine serum albumin (BSA), APTES and sodium borohydride ($NaBH_4$) were from Sigma-Aldrich Chemical (St. Louis, USA, www.sigmaaldrich.com). L-cysteine was obtained from Aladdin Biochemical Technology Co., Ltd. (Shanghai, China, www.aladdin-e.com). H_2O_2 was obtained from Chongqing Chuandong Chemical Group Co., Ltd. (Chongqing, China). Lead Standard Solution, Magnesium Standard Solution and the other metal ions' Standard Solution were obtained from ZONO Biotechnology Co. (Chongqing, China). All DNA oligonucleotides used in this work were supplied by Sangon Biotech Co., Ltd. (Shanghai, China). Their sequences are provided in Table S1.

The buffer solutions employed in this experiment were as follows: 10 mM Tris-HCL buffer (pH 7.4) containing 1 mM EDTA, 1 mM $CaCl_2$, 5 mM KCl, and 0.1 M NaCl, which was used to dissolve Bio-ES. Hybridization buffer (10 mM Tris-HCL, 0.1 M NaCl, 1 mM EDTA and 5 mM $MgCl_2$, pH 7.4) was used to prepare solutions for SS, G-DNA and Helper DNA. Phosphate-buffered saline (PBS, pH 6.8) containing 0.1 M Na_2HPO_4, 0.1 M KH_2PO_4 and 0.1 M KCl was used as the working buffer. All other chemical reagents were of analytical grade and were used without any purification or treatment. Ultrapure distilled and deionized water (18.2 MΩ) obtained from a Millipore Mill-Q purification system was used for all solution preparations. A description and characterization of the apparatus were shown in detail in Supplementary information S1.

2.2. Preparation of the APTES-functionalized rGO-SnO_2

Preparation of the APTES-functionalized rGO-SnO_2 (APTES-rGO-SnO_2) was performed following procedures reported in a previous study with minor changes (Xu et al., 2018b). First, 0.1 g of rGO-SnO_2 composites were dispersed in 25 mL ethanol and ultrasonicated for at least 30 min to form symmetrical dispersions. Second, obtained dispersions were mixed with 0.1 mL APTES and stirred at 70 °C for 1.5 h. Third, obtained APTES-rGO-SnO_2 mixtures were purified by centrifugation at 8000 rpm for 5 min and washed three times with ultrapure water at room temperature. Finally, the prepared products were dried at 65 °C. Subsequently, 3.5 mg of APTES-rGO-SnO_2 was dispersed in 1 mL of ultrapure water and ultrasonicated to obtain a homogeneous solution.

2.3. Synthesis of MoS_2–AuPt, MoS2–Au, MoS_2–Pt and AuNPs

Preparation of L-cysteine-functionalized MoS_2 was conducted by following procedures reported in a previous method with minor modifications (Ji et al., 2018).

Briefly, 10 mg of MoS_2 nanosheets were dispersed in 10 mL

ultrapure water and ultrasonicated for at least 20 min to form symmetrical dispersions. Then, 100 μL of 50-mM aqueous L-cysteine solution was added into the above solution and ultrasonicated for 30 min. Next, 1 mL of the obtained solution was mixed with 200 μL of 1% $HAuCl_4{\cdot}4H_2O$ and 200 μL of 1% $H_2PtCl_6{\cdot}6H_2O$. After ultrasonicating for 20 min, 2 mL of 0.1 M $NaBH_4$ solution was added dropwise into the mixture under ultrasonication. The MoS_2–AuPt product was collected by centrifugation and washing with ultrapure water three times, followed by drying in a vacuum at 65 °C. Finally, 2 mg MoS_2–AuPt was dispersed in 1 mL ultrapure water and kept at 4 °C for further use. Detailed procedures for the synthesis of MoS_2–Au, MoS_2–Pt and AuNPs were provided in Supplementary information S2.

2.4. Preparation of Pb^{2+} DNAzyme and G-DNA labeled MoS_2–AuPt nanocomposites (signal labels)

First, 20 μL of 10-μM Bio-ES and 20 μL of 10-μM SS were mixed with 160 μL of 20-mM Tris-HCL buffer (pH 7.4) to form Pb^{2+} DNAzyme. Then, the mixture was reacted at 65 °C for 10 min, followed by cooling to room temperature. For further hybridization, the solution was gently shaken at room temperature for 12 h. Subsequently, the Bio-ES-SS solution was stored at 4 °C when not in use.

In order to amplify the electrochemical signal and enhance the sensitivity of the electrochemical biosensor, G-DNA labeled MoS_2–AuPt nanocomposites was used as a signal enhancer. Briefly, 1 mL prepared MoS_2–AuPt (2 mg mL^{-1}) nanocomposites was mixed with 100 μL of 2-μM G-DNA, followed by gentle stirring at 4 °C for 12 h. Next, G-DNA was attached onto the MoS_2–AuPt surface through Au–NH_2 bond or Pt–NH_2 bond. To block nonspecific adsorption sites, 50 μL BSA (w/w, 1%) was introduced to the mixture for 30 min. Unbound G-DNA was removed by centrifugation at 8000 rpm for 5 min and washing with ultrapure water three times. Finally, the obtained product was dispersed in 1 mL hybridization buffer and kept at 4 °C for further use.

2.5. Fabrication of the proposed electrochemical biosensor

The fabrication process for the proposed Pb^{2+} biosensor is outlined in Scheme 1.

Prior to modification, a bare GCE was polished repeatedly with 0.3 μm and 0.05 μm alumina slurries to a mirror. Then, GCE was rinsed ultrasonically with ultrapure water, anhydrous ethanol and ultrapure water for 5 min in sequence.

After drying the GCE in nitrogen at room temperature, 3.0 mg mL^{-1} of the APTES-rGO-SnO_2 solution was dropped onto the cleaned GCE surface and air-dried. Then, 10 μL AuNPs was loaded onto the resulting electrode surface via Au–NH_2 bonds. When the electrode dried, 10 μL of 1.5 μg mL^{-1} SA was coated onto the modified electrode and kept at 4 °C for 12 h, allowing the SA to combine with the AuNPs via Au–NH_2 bonds. After the reaction, the electrode was thoroughly washed with a PBS (pH 6.8, 0.2 M) to remove loosely bound reactants and was then dried in nitrogen. Next, 10 μL of 1-μM Bio-ES-SS solution was added onto the prepared electrode and incubated at 4 °C for 3 h, resulting in immobilization of Bio-ES-SS on the electrode through the streptavidin-biotin affinity (Zhang et al., 2018). To block nonspecific binding, 10 μL BSA solution (w/w, 1%) was used to cover the surface of the electrode and incubated at room temperature for 30 min. Finally, the resulting biosensor was prepared for electrochemical analysis.

2.6. Electrochemical measurement

Initially, 10 μL Pb^{2+} standard solutions with different concentrations were dropped onto the modified electrode and reacted for 90 min at room temperature. In the presence of Pb^{2+}, the Pb^{2+} DNAzyme was activated, and Pb^{2+} specifically identified and cleaved the SS into two fragments at the 'rA' site, followed by release of the ES. Next, 10 μL of 2 μM Helper DNA was immobilized onto the resulting electrode to hybridize with the exposed ES for 30 min. When washing with PBS, 10 μL G-DNA labeled MoS_2–AuPt nanocomposites was coated onto the prepared electrode for 1 h to achieve electrochemical signal amplification. Following that, 2 μM hemin was added onto the electrode and incubated for 30 min at room temperature to form the hemin/G-quadruplex. After every modification on the biosensor, the electrode surface was washed with PBS, then subjected to electrochemical measurements.

All electrochemical measurements were conducted in an electrochemical workstation with a conventional three-electrode system. The CV and EIS measurements were both executed step by step in a 5 mM $[Fe(CN)_6]^{3-/4-}$ solution including 0.1 M KCl. The CV measurements were carried out by scanning from −0.2 V to +0.6 V at a scan rate of 100 mV s^{-1}; The EIS parameters contained a 10 mV amplitude and a frequency sweep range of 0.1 to 105 Hz at room temperature. To perform the electrochemical measurement, the amperometric i-t curves were recorded at −0.4 V in 10 mL detection solution (PBS, pH 6.8) at room temperature. After the background current was stable, 10 μL of 3.3-M H_2O_2 was added into the solution, and the electrochemical signal changes were recorded.

3. Result and discussion

3.1. Characterization of different nanomaterials

The morphology and size of the synthesized nanocomposite was characterized by FE-SEM. As shown in Fig. 1A, the surface morphology of the MoS_2 nanosheet was a single-layer or few-layer structure, illustrating the unique layered structures of MoS_2. After the MoS_2 was modified with AuPt-NPs by in situ reduction of $HAuCl_4$ and H_2PtCl_6, AuPt-NPs with diameters of approximately 250-350 nm were uniformly distributed on the surface of MoS_2 nanosheets at a high density, indicating that the MoS_2–AuPt nanocomposites had successfully been synthesized (Fig. 1B). Meanwhile, the characterization (Fig. S1) of rGO-SnO_2 and AuNPs are described in Supplemental Information S3. In addition, AFM characterization results are shown from Fig. S2. As shown in Fig. S2A, the mean roughness of MoS_2 nanosheet was 0.605 nm, which increased to 28.296 nm after the MoS_2 nanosheet modificated successfully with AuPt-NPs (Fig. S2B). The results of AFM characterization are in accordance with the above FE-SEM characterization method.

Additionally, EDS and XPS were applied for elemental analysis to further confirm synthesis of the MoS_2–AuPt nanocomposites. Examination of the EDX image (Fig. 1C) illustrates that characteristic elements of Mo, S, Au and Pt are observed, implying successful loading of AuPt-NPs onto the MoS_2 nanosheet. In addition, characteristic peaks for the Mo3d, S2p, Au4f, and Pt4f core level regions were clearly obtained in the MoS_2–AuPt nanocomposites from the XPS image (Fig. 1D). The spectra of Mo3d, S2p, Au4f, and Pt4f were shown in Fig. 1E, F, G and H and were consistent with the previous report. Moreover, elemental mapping was also employed to investigate the elemental composition of the MoS_2–AuPt nanocomposites, and characteristic signals for the Mo, S, Au and Pt elements are all clearly observed in Fig. S3. Taken together, these results prove that the MoS_2–AuPt nanocomposites were successfully synthesized.

3.2. Electrochemical behavior of the stepwise-modified electrode

To characterize the fabrication process (Scheme 1) of the proposed electrochemical Pb^{2+} biosensor, the assembly steps of the sensing interface were investigated using EIS and CV measurements after each incubation step. The CVs of different modified electrodes were monitored in a 5 mM $[Fe(CN)_6]^{3-/4-}$ solution containing 0.1 M KCl at a scan rate of 100 m V·s^{-1} at room temperature. As shown in Fig. 2A, with the reversible redox reaction of ferricyanide ions on the surface of the bare GCE, a pair of well-defined redox peaks (+79.691 μA; -72.706 μA) were

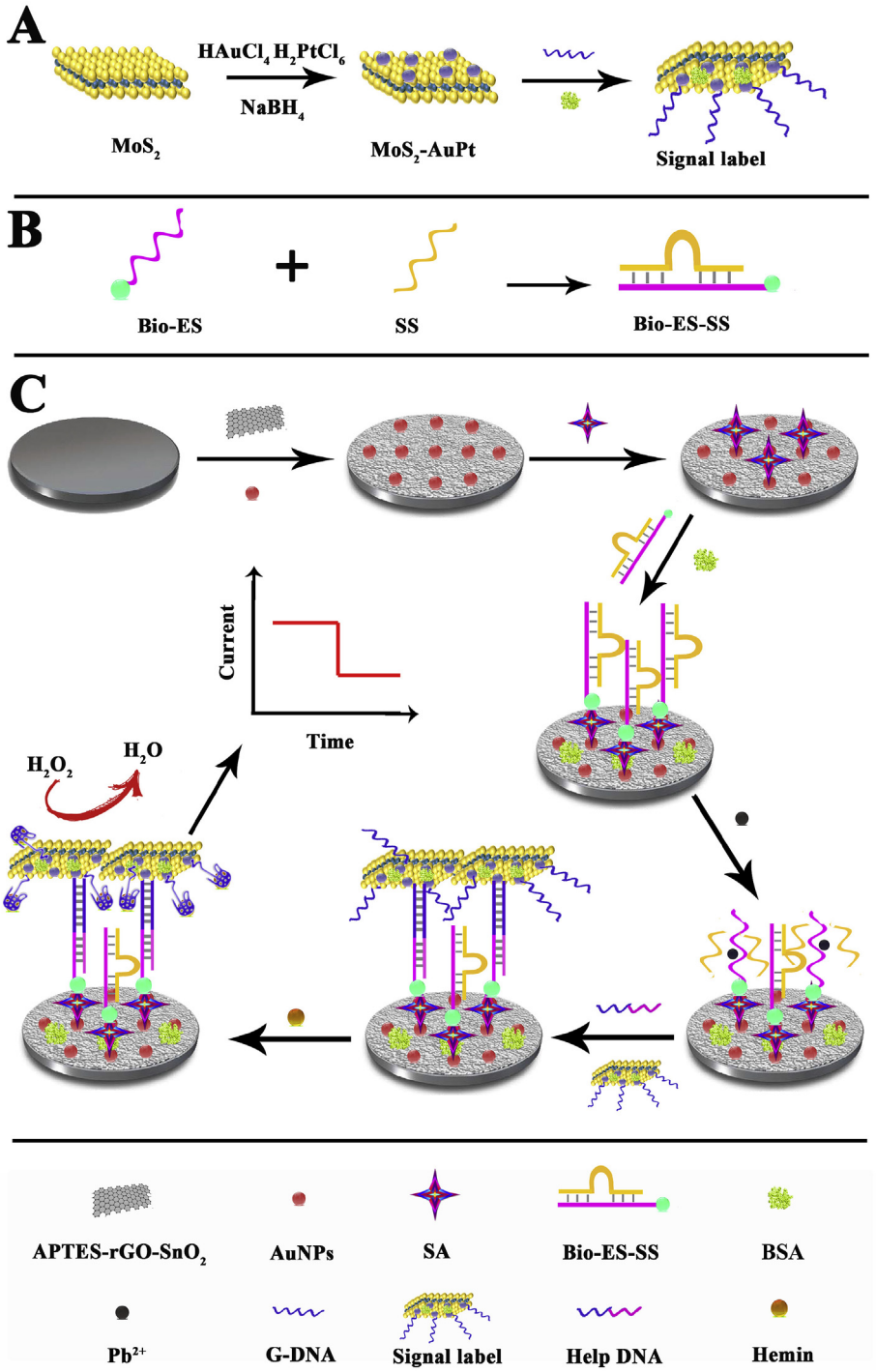

Scheme 1. Schematic representation of stepwise electrochemical biosensor fabrication process for Pb^{2+} detection.

observed (curve a). When the GCE was coated with APTES-rGO-SnO_2, the peak CV current (+103.24 μA; -113.3 μA) visibly increased (curve b), indicating that the APTES-rGO-SnO_2 have excellent electrical conductivity. After adding AuNPs on the APTES-rGO-SnO_2/GCE surface, the peak current (+163.88 μA; -167.05 μA) of the Au/APTES-rGO-SnO_2/GCE increased markedly (curve c), owing to the fact that AuNPs accelerate electron transfer. Next, the peak current (+112.52 μA; -117.91 μA) decreased sharply after SA was captured on the surface of the modified electrode (curve d) due to the poor conductivity of streptavidin. When the Bio-ES–SS–based Pb^{2+} specific DNAzyme immobilized onto the SA/Au/APTES-rGO-SnO_2/GCE, a decreased peak current (+98.915 μA; -101.1 μA) was clearly observed (curve e) as the double-stranded DNA hindered electron transfer. As expected, non-conductive BSA, utilized as a blocking agent, blocked nonspecific active sites on the Bio-ES-SS/SA/Au/APTES-rGO-SnO_2/GCE and produced another decrease of the peak current (+65.316 μA; -73.328 μA) (curve f). With the final introduction of 100 ng mL^{-1} Pb^{2+} standard solution on the BSA/Bio-ES-SS/SA/Au/APTES-rGO-SnO_2/GCE, the redox peak current (+86.381 μA; -96.08 μA) increased (curve g), demonstrating that Pb^{2+}-dependent specific DNAzyme identified and cleaved its substrate at 'rA' into two fragments. Because the negatively charged DNA backbones decreased from the electrode surface, the obstacle of DNAzyme to electron transfer was reduced. These results demonstrate that each step in the fabrication of the biosensor was successful.

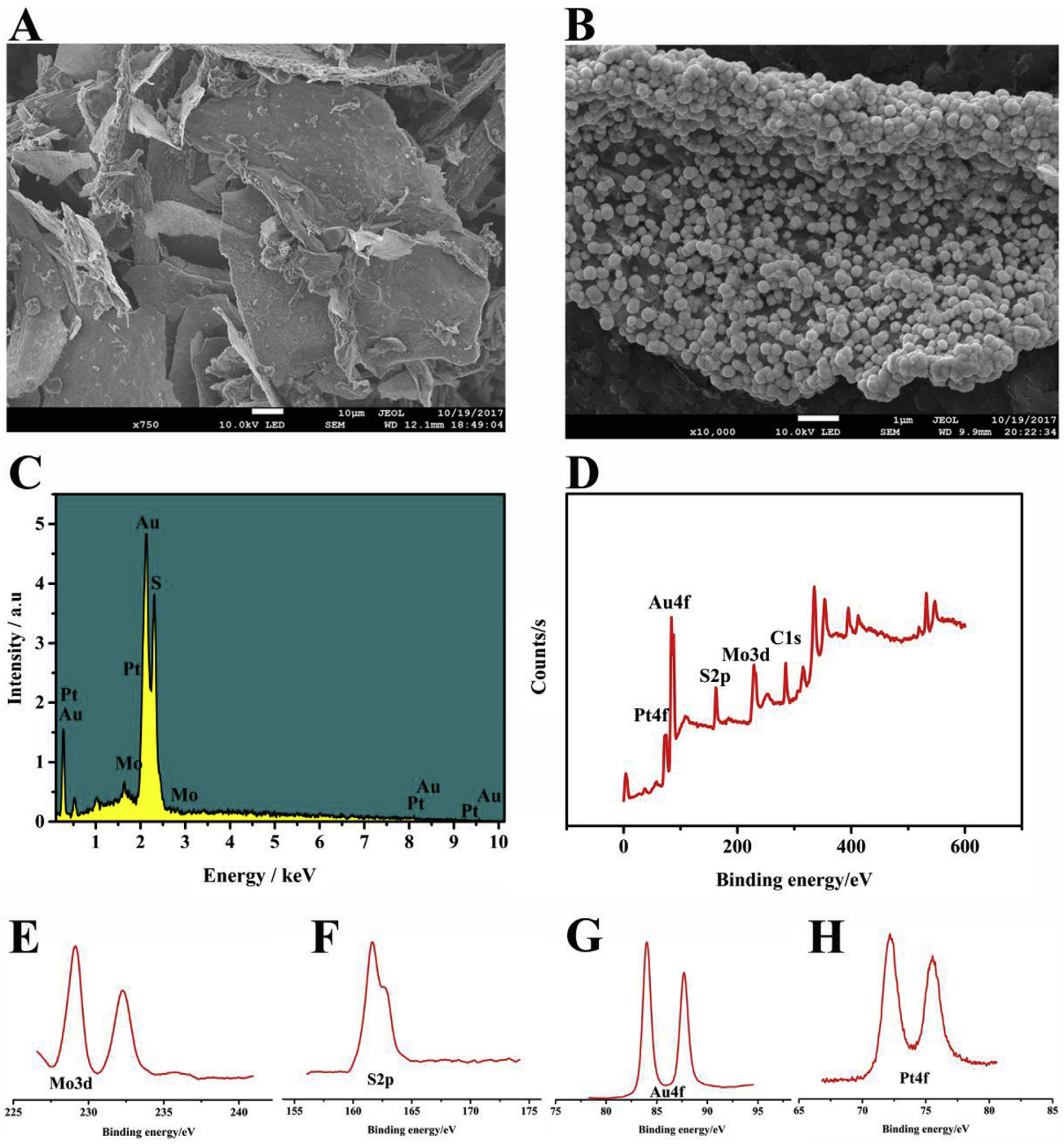

Fig. 1. FE-SEM image of **(A)** the MoS_2 nanosheets and **(B)** the MoS_2–AuPt nanocomposites. EDS of the MoS_2–AuPt nanocomposites **(C)**. The XPS spectrum of the MoS_2–AuPt nanocomposites **(D)**. Spectra of Mo3d in the MoS_2–AuPt nanocomposites **(E)**, S2p in the MoS_2–AuPt nanocomposites **(F)**, Au4f in the MoS_2–AuPt nanocomposites **(G)** and Pt4f in the MoS_2–AuPt nanocomposites **(H)**.

In addition, EIS was employed to further verify the stepwise processes of the modified electrode in a 5 mM $[Fe(CN)_6]^{3-/4-}$ solution containing 0.1 M KCl. In the Nyquist diagram, the semicircle diameter equals that of the electron transfer resistance (Ret), and the linear section of the curve at low frequency represents the diffusion process (Chen et al., 2017a). As shown in Fig. 2B, when APTES-rGO-SnO_2 was coated onto the bare electrode, the resistance decreased (curve b) compared to the bare GCE (curve a) because APTES-rGO-SnO_2 accelerates electron transfer of the electrode. After AuNPs were dropped onto the electrode, the diameter of the semicircle was clearly decreased (curve c), indicating that AuNPs enhance electron transfer between the electrode and the solution. Upon the addition of SA onto the modified electrode, the semicircle diameter noticeably increased (curve d), proving that nonconductive SA hinders electron transfer and was successively immobilized onto the electrode. Additionally, incubation of the Bio-ES–SS–based Pb^{2+} specific DNAzyme on the electrode resulted in the resistance increasing significantly (curve e) owing to the resistance of $[Fe(CN)_6]^{3-/4-}$ approaching the electrode by the negatively charged DNA backbones. Later, adding nonconductive BSA as a blocking agent caused the resistance to increase further (curve f). In contrast, the semicircle diameter decreased after the resultant electrode reacted with target Pb^{2+} (curve g), suggesting that Pb^{2+}-dependent

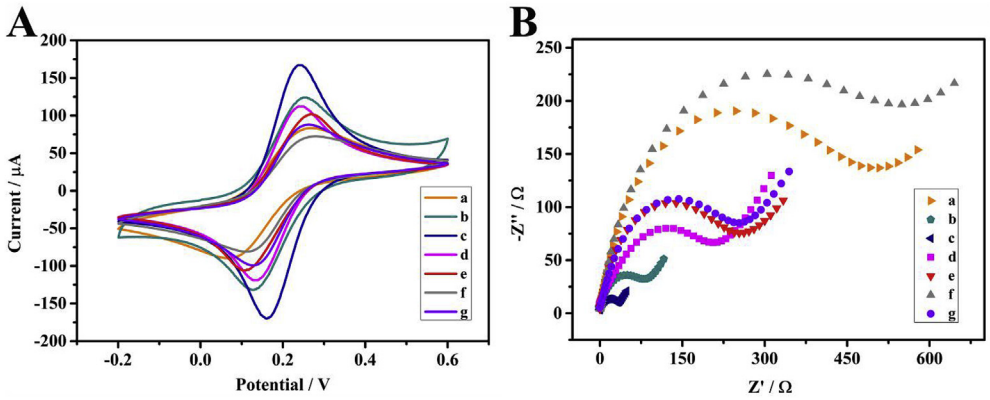

Fig. 2. (A) CV and **(B)** EIS characterization of electrodes at various stages of modification in a 5 mM $[Fe(CN)_6]^{3-/4-}$ solution: (a) bare GCE, (b) APTES-rGO-SnO_2/GCE, (c) Au/APTES-rGO-SnO_2/GCE, (d)SA/Au/APTES-rGO-SnO_2/GCE, (e) Bio-ES-SS/SA/Au/APTES-rGO-SnO_2/GCE, (f) BSA/Bio-ES-SS/SA/Au/APTES-rGO-SnO_2/GCE, (g) Pb^{2+}/BSA/Bio-ES-SS/SA/Au/APTES-rGO-SnO_2/GCE.

DNAzyme acquired its cleavage activity and cleaved the substrate strand in the presence of Pb^{2+}. All of these results further verified the successful fabrication of the designed biosensor.

3.3. The electrochemical behaviour of different substrate nanomaterials and signal nanomaterials

The amperometric i-t curve was applied to compare the electrochemical behaviours of different substrate nanomaterials and signal nanomaterials (Fig. 3). All assay procedures were implemented with the same concentration of target Pb^{2+} (100 ng mL^{-1}). As shown in Fig. 3A, compared to the biosensor incubated with substrate nanomaterials APTES-rGO, APTES-rGO-SnO_2 showed a clear increase in the electrochemical signal because APTES-rGO-SnO_2 has an excellent ability to accelerate electron transfer. Additionally, the electrochemical signal remarkably increased when the biosensor was incubated with the signal amplification tag MoS_2–Pt-G-DNA-BSA compared to the MoS_2–Au-G-DNA-BSA (Fig. 3B) owing to the catalytic ability of PtNPs being stronger than AuNPs. In addition, when MoS_2–AuPt-G-DNA-BSA was applied as a signal amplification tag to modify the electrode, the biosensor exhibited a much greater electrocatalytic current response than in the case of PtNPs (Fig. 3C) due to AuPt-NPs' ability to synergistically catalyze the reduction of H_2O_2 to increase the electrochemical signal. Notably, the electrochemical signal further increased (Fig. 3D) when the hemin/G-quadruplex was utilized to label the MoS_2–AuPt, likely due to hemin/G-quadruplexes mimicking peroxidase and MoS_2–AuPt nanocomposites having cocatalysis ability, which amplified the electrochemical signal. As shown in Fig. 3E, the current was clearly increased when the biosensor was combined with the biotin-streptavidin system due to the biotin-streptavidin system possessing the highest known affinity in nature (Jiang et al., 2011). Comparison of all results demonstrates that our proposed electrochemical biosensor significantly improves sensitivity for Pb^{2+} detection.

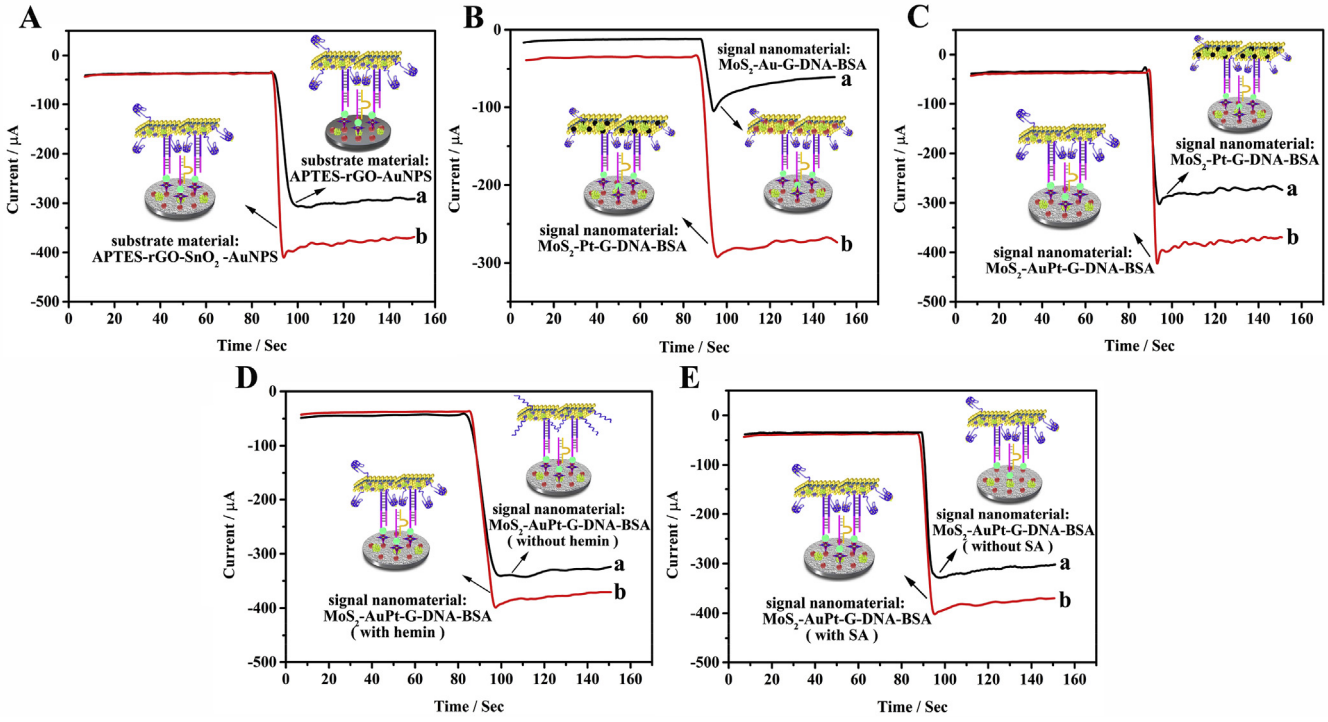

Fig. 3. The i-t curve of the prepared electrochemical biosensor incubated with different nanomaterials: **(A)** substrate material: APTES-rGO-AuNPs (a) and APTES-rGO-SnO_2-AuNPs (b); **(B)** signal material: MoS_2–Au-BSA-G-DNA (a) and MoS_2–Pt-BSA-G-DNA (b); **(C)** signal material: MoS_2–Pt-BSA-G-DNA (a) and MoS_2–AuPt-BSA-G-DNA (b); **(D)** signal material: MoS_2–AuPt-BSA-G-DNA (without hemin, a) and MoS_2–AuPt-BSA-G-DNA (with hemin, b); and **(E)** signal material: MoS_2–AuPt-BSA-G-DNA (without SA, a) and MoS_2–AuPt-BSA-G-DNA (with SA, b).

3.4. Optimization of the experimental conditions

The electrochemical signal of the proposed biosensor is influenced by many experimental conditions. To achieve optimal biosensor response, several critical parameters were optimized: (a) concentration of APTES-rGO-SnO_2; (b) concentration of SA; (c) concentration of Bio-ES-SS; (d) immobilization time of Bio-ES-SS; (e) cleavage time of Pb^{2+}-dependent specific DNAzyme; (f) concentration of hemin; (g) volume of 1% $HAuCl_4{\cdot}4H_2O$ and 1% $H_2PtCl_6{\cdot}6H_2O$; (h) concentration of MoS_2–AuPt nanocomposites; and (i) pH value. These results (Fig. S4) were described in Supplemental Information S4. In addition, the following experimental conditions yielded satisfactory results: (a) APTES-rGO-SnO_2 concentration of 3.0 mg mL^{-1}; (b) SA concentration of 1.5 μg mL^{-1}; (c) Bio-ES-SS concentration of 1 μM; (d) Bio-ES-SS immobilization time of 3 h; (e) Pb^{2+}-dependent specific DNAzyme cleavage time of 90 min; (f) hemin concentration of 2.5 μM; (g) 1% $HAuCl_4{\cdot}4H_2O$ and 1% $H_2PtCl_6{\cdot}6H_2O$ volume of 200 μL; (h) MoS_2–AuPt nanocomposites concentration of 2.0 mg mL^{-1}; and (i) pH of 6.8.

3.5. Analytical performance of the proposed electrochemical biosensor

Under optimized conditions, the effects of different concentrations of target Pb^{2+} on H_2O_2-catalytic ability were recorded using an amperometric i-t curve at −0.4 V in 10 mL of PBS (pH 6.8). The relationship between the various electrochemical signals and targeted Pb^{2+} at concentrations ranging from 0.1 pg mL^{-1} to 1000 ng mL^{-1} was shown in Fig. 4A. The i-t curve gradually increased as Pb^{2+} concentration increased. Additionally, it is clear that the current response shows good linear increase with the logarithm of Pb^{2+} concentrations, as shown in Fig. 4B and as expressed by the linear eq. $Y = 21.918*\log C_{Pb}{}^{2+} + 223.6$ (pg·mL^{-1}) with $R^2 = 0.9978$. In addition, the limit of detection (LOD) was calculated to be 38 fg mL^{-1} (based on 3σ), which was obviously better than those for previously reported methods for Pb^{2+} detection, as shown in Table S2. The low detection limit may be attributed to several factors. First, the APTES-rGO-SnO_2 /Au serves as a sensor platform for immobilizing more Pb^{2+}-specific DNAzyme with high conductivity. Second, the use of Pb^{2+}-specific DNAzyme strengthened the selectivity of the biosensor, and the use of the biotin-streptavidin system improved the sensitivity of the proposed biosensor. Third, utilization of the MoS_2–AuPt nanocomposites and hemin/G-quadruplex DNAzyme further enhanced the electrochemical signal, leading to higher sensitivity. Therefore, the proposed strategy for Pb^{2+} detection based on DNAzymes and MoS_2–AuPt nanocomposites exhibits a very low detection limit.

3.6. Specificity, repeatability and stability of the proposed biosensor

There may be various species of metal pollutants in the water environment. To determine high specificity of the proposed biosensor in distinguishing target Pb^{2+} from other metal ions, we chose 7 kinds of metal ions to use as interference (K^+, Mg^{2+}, Cu^{2+}, Ca^{2+}, Zn^{2+}, Mn^{2+}, and Cd^{2+}). Specificity was investigated with Pb^{2+} (100 ng mL^{-1}),

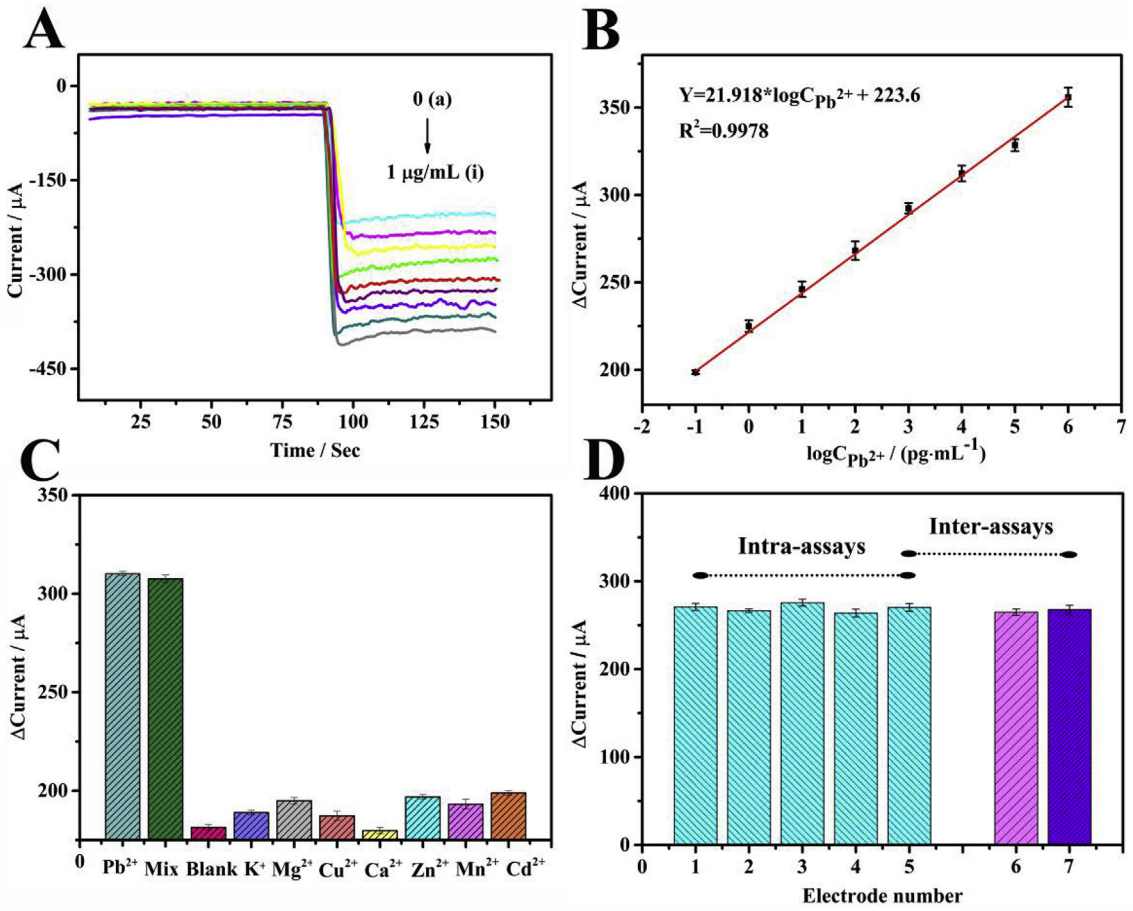

Fig. 4. (A) The i-t curve signals of the proposed biosensor for detection of different concentrations of Pb^{2+}: (a) 0 pg mL^{-1}, (b) 0.1 pg mL^{-1}, (c) 1 pg mL^{-1}, (d) 10 pg mL^{-1}, (e) 100 pg mL^{-1}, (f) 1 ng mL^{-1}, (g) 10 ng mL^{-1}, (h) 100 ng mL^{-1}, (i) 1000 ng mL^{-1}. **(B)** Calibration curve of the proposed biosensor for different concentrations of Pb^{2+} (n = 3). **(C)** Specificity of the proposed biosensor for 100 ng mL^{-1} of Pb^{2+} against the zero analyte (Blank); other interference metal ions with the same concentration of 1 μg mL^{-1}: K^+, Mg^{2+}, Cu^{2+}, Ca^{2+}, Zn^{2+}, Mn^{2+}, Cd^{2+} and their mixture with 100 ng mL^{-1} of Pb^{2+}(Mix). **(D)** Reproducibility of 7 different electrodes modified with 1 ng mL^{-1} of Pb^{2+}.

Table 1
Statistical analysis of Pb^{2+} determination in water environment with AAS method and the proposed biosensor.

Sample	Sample number	AAS (ng·mL^{-1})	This work ($\bar{x}$, ng·mL^{-1})	Error	Rank
tap water	1	0.68	0.69	+0.01	1
	2	0.68	0.66	−0.02	−2.5
pool water	3	1.12	1.18	+0.06	5
	4	1.25	1.20	−0.05	−4
lake water	5	0.26	0.28	+0.02	2.5
	6	0.26	0.26	0	
					$T_+ = 8.5$
					T- = 6.5
P > 0.05					

interference (1 μg mL^{-1}) and the mixture (composed of the 1 μg mL^{-1} interference ions and 100 ng mL^{-1} Pb^{2+}) at the same optimal experimental conditions. Fig. 4C displays the current responses for Pb^{2+}, the Mix, a blank and seven kinds of interferences. Even in the presence of 10-fold higher concentrations of interference ions compared to target Pb^{2+}, they had almost no effect on current response compared to the blank assay. In addition, current response was not significantly different between target Pb^{2+} and the Mix. Therefore, the proposed biosensor exhibited high specificity for Pb^{2+} detection.

Next, intra- and interassay repeatability of the electrochemical biosensor was examined by repeatedly measuring the same concentration of Pb^{2+}, as shown in Fig. 4D. Intra- and interassay relative standard deviation (RSD) values were 1.39% and 1.59%, respectively. These results revealed that the assembled biosensor exhibits acceptable repeatability. Additionally, to investigate the stability of the proposed biosensor, the fabricated electrochemical biosensor was stored at 4 °C before use. There were no obvious differences during the first 5 days of storage, and the current changes were less than 2.23%. After 20 days of storage, the designed biosensor retained 88.43% of its initial current response (Fig. S5), indicating that the proposed biosensor offers satisfactory stability for Pb^{2+} detection. Moreover, a analytical performance comparison between this designed electrochemical biosensor and the other detection methods in recent years is demonstrated in Table S2.

3.7. Analysis of real samples

3.7.1. Detection performance in water samples

To evaluate the performance of this method in practical applications, the fabricated electrochemical biosensor was used to detect Pb^{2+} in water samples. Different concentrations of the Pb^{2+} standard solution were added to the water samples to calculate the recovery rate by amperometric i-t curves under optimal experimental conditions. As shown in Table S3, recoveries of Pb^{2+} ranged from 92.40% to 104.95% for all samples. In addition, accuracy was evaluated by the RSD of 1.24%–2.25%. These results indicate that this electrochemical method exhibits satisfactory precision for Pb^{2+} detection.

3.7.2. Pb^{2+} determination in the real samples

To demonstrate the application potential of this biosensor using real samples, the developed biosensor was used to assay Pb^{2+} in fresh tap water, pool water and lake water, which were obtained from the lab, a pool located in the campus of Chongqing Medical University (Chongqing, China) and local Caiyun Lake (Chongqing, China), respectively. The tap water was used without any treatment, and the pool water and lake water were centrifuged at 12,000 rpm for 10 min. AAS was applied at the same time as verification for each sample. As shown in Table S4, results demonstrated that this electrochemical method is applicable for detection of Pb^{2+} in environmental water samples.

3.7.3. Statistical analysis

To further testify the difference in results, which was caused by the detection method, it is necessary to adopt hypothesis testing using a statistical method. The Wilcoxon signed-rank test was applied to analyze the six water samples (1-6) as shown in Table 1, SPSS20 software was used to calculate data with $Z = -0.271$, $P = 0.786$, $P > 0.05$ ($P < 0.05$ is considered statistically significant). These results demonstrate that there is no statistically significant difference between the application of AAS and the designed biosensor method, indicating that detection results of AAS and the detection results of the designed biosensor method are indistinguishable. Thus, the designed sensing platform is potentially applicable for detection of target Pb^{2+} in a water environment.

4. Conclusion

Herein, an efficient electrochemical biosensor was developed for Pb^{2+} detection. In this method, Pb^{2+}-dependent DNAzyme was applied to strengthen the selectivity of the electrochemical biosensor; MoS_2–AuPt nanocomposites displayed excellent electrocatalytic activity due to their structural advantages and highly conductivity, and hemin/G-quadruplex-based DNAzyme-labeled MoS_2–AuPt enhanced sensitivity of the biosensor as a signal label. Furthermore, use of APTES-rGO-SnO_2, AuNPs and the SA system enabled a large surface area and superior conductivity for the biosensor. With these advantages, this biosensor design exhibited extremely low LOD, a wide detection range, excellent selectivity, acceptable reproducibility and stability and can be used for Pb^{2+} detection in the water environment. However, this proposed strategy could not be adapted for analyzing other metal ions (e.g., Hg^{2+}, Cu^{2+}, Cd^{2+}), which is a limitation in this method. In the future work, we will overcome this drawback and extend our strategy to detect other metal ions by applying their appropriate respective metal ion-dependent DNAzymes, thus representing a promising platform for the development of electrochemical biosensors.

Acknowledgements

This research was supported by the National Natural Science Foundation of China (Grant Nos. 31071093, 31170129, and 31200064) and the Science and Technology Planning Project of Yuzhong District of Chongqing City, China (No. 20140119).

Appendix A. Supplementary data

Supplementary data to this article can be found online at https://doi.org/10.1016/j.bios.2019.111560.

References

Behbahani, M., Hassanlou, P.G., Amini, M.M., Omidi, F., Esrafili, A., Farzadkia, M., Bagheri, A., 2015. Food Chem. 187, 82–88.
Bingqian, L., Yuling, C., Dianping, T., Huanghao, Y., Guonan, C., 2012. Chem. Commun. 48, 2624–2626.
Bleul, A., Dieckmann, C., Geissler, M., Gruber, G., Leberwurst, K., Lindner, K., Wohlbold, L., 2016. Talanta 146, 641–647.
Chen, J., Yu, C., Zhao, Y., Niu, Y., Zhang, L., Yu, Y., Wu, J., He, J., 2017a. Biosens. Bioelectron. 91, 892–899.
Chen, S., Liu, P., Su, K., Li, X., Qin, Z., Xu, W., Chen, J., Li, C., Qiu, J., 2017b. Biosens. Bioelectron. 99, 338–345.
Cui, M., Huang, J., Wang, Y., Wu, Y., Luo, X., 2015. Biosens. Bioelectron. 68, 563–569.
Dong, J., Fang, Q., He, H., Zhang, Y., Xu, J., Sun, Y., 2015. Microchimica Acta 182, 653–659.
Feng, W., Runjhun, S., Juewen, L., 2015. Bioorg. Med. Chem. Lett 25, 1460–1463.
Gang, L., Yan, M., An, L., Jin, X., Liu, X., Pan, L., 2017. Microchem. J. 131, 145–153.
Gao, F., Fan, T., Wu, J., Liu, S., Du, Y., Yao, Y., Zhou, F., Zhang, Y., Liao, X., Geng, D., 2017. Biosens. Bioelectron. 96, 62–67.
Guo, L., Nie, D., Qiu, C., Zheng, Q., Wu, H., Ye, P., Hao, Y., Fu, F., Chen, G., 2012. Biosens. Bioelectron. 35, 123–127.
He, Y., Wang, X., Zhang, Y., Gao, F., Li, Y., Chen, H., Wang, L., 2013. Talanta 116, 816–821.
Huang, X., Li, J., Zhang, Q., Shuai, C., Wei, X., Wu, J., Niu, W., Xue, J., Li, C., 2018. J.

Electroanal. Chem. 816, 75–82.
Huang, Y., Zheng, J., Wang, L., Duan, X., Wang, Y., Xiang, Y., Li, G., 2019. Biosens. Bioelectron. 127, 45–49.
Ji, R., Chen, S., Xu, W., Qin, Z., Qiu, J.F., Li, C.R., 2018. Mikrochim. Acta 185, 209.
Jiang, X., Chen, K., Han, H., 2011. Biosens. Bioelectron. 28, 464–468.
Li, S., Wang, Y., Lai, C., Qiu, J., Ling, M., Martens, W., Zhao, H., Zhang, S., 2014a. J. Mater. Chem. 2, 10211–10217.
Li, W., Yang, Y., Chen, J., Zhang, Q., Wang, Y., Wang, F., Yu, C., 2014b. Biosens. Bioelectron. 53, 245–249.
Liu, S., Wei, W., Sun, X., Wang, L., 2016. Biosens. Bioelectron. 83, 33–38.
Liu, S., Yang, Z., Chang, Y., Chai, Y., Yuan, R., 2018. Biosens. Bioelectron. 119, 170–175.
Murali, K.S., Kempahanumakkagari, S.K., Varley, T.S., Nagaraju, D.H., Ramakrishnappa, T., 2014. Anal. Methods 6, 8698–8705.
Shamsipur, M., Farzin, L., Tabrizi, M.A., Sheibani, S., 2017. Mater. Sci. Eng. C 77, 459–469.
Sun, Q., Wang, J., Tang, M., Huang, L., Zhang, Z., Liu, C., Lu, X., Hunter, K.W., Chen, G., 2017. Anal. Chem. 89, 5024–5029.
Vishnu, N., Badhulika, S., 2019. Biosens. Bioelectron. 124-125, 122–128.
Wang, L.L., Wen, Y., Li, L., Yang, X., Jia, N., Li, W., Meng, J., Duan, M., Sun, X., Liu, G., 2018. Biosens. Bioelectron. 115, 91–96.
Wang, H., Zhu, L., Duan, J., Wang, M., Yin, H., Wang, P., Ai, S., 2018a. Biosens. Bioelectron. 103, 32–38.
Wang, X., Wang, M., Zhang, Y., Miao, X., Huang, Y., Zhang, J., Sun, L., 2016. Biosens. Bioelectron. 83, 91–96.
Wang, X.Y., Niu, C.G., Guo, L.J., Hu, L.Y., Wu, S.Q., Zeng, G.M., Li, F., 2017. J. Fluoresc. 27, 643–649.
Wang, Z., Li, J., Xu, L., Feng, Y., Lu, X., 2014. J. Solid State Electrochem. 18, 2487–2496.
Xu, S., Chen, X., Peng, G., Jiang, L., Huang, H., 2018a. Anal. Bioanal. Chem. 410, 1–9.
Xu, W., Qin, Z., Hao, Y., He, Q., Chen, S., Zhang, Z., Peng, D., Wen, H., Chen, J., Qiu, J., 2018b. Biosens. Bioelectron S095656631830349X.
Xue, S., Jing, P., Xu, W., 2016. Biosens. Bioelectron. 86, 958–965.
Yang, Y., Yuan, Z., Liu, X.P., Liu, Q., Mao, C.J., Niu, H.L., Jin, B.K., Zhang, S.Y., 2016. Biosens. Bioelectron. 77, 13–18.
Yang, Z., Zhuo, Y., Yuan, R., Chai, Y., 2015. ACS Appl. Mater. Interfaces 7.
Yin, H.S., Li, B.C., Zhou, Y.L., Wang, H.Y., Wang, M.H., Ai, S.Y., 2017. Biosens. Bioelectron. 96, 106–112.
Yu, J., Yang, S., Lu, Q., Sun, D., Zheng, J., Zhang, X., Wang, X., Yang, W., 2017. Talanta 164, 216.
Zhang, B., Chen, J., Liu, B., Tang, D., 2015a. Biosens. Bioelectron. 69, 230–234.
Zhang, K., Liu, G., Goldys, E.M., 2018. Biosens. Bioelectron. 102, 80–86.
Zhang, Y., Fan, J., Nie, J., Le, S., Zhu, W., Gao, D., Yang, J., Zhang, S., Li, J., 2015b. Biosens. Bioelectron. 73, 13–18.
Zhao, J., Shu, D., Ma, Z., 2019. Biosens. Bioelectron. 127, 161–166.
Zhou, Q., Lin, Y., Lin, Y., Wei, Q., Chen, G., Tang, D., 2016. Biosens. Bioelectron. 78, 236–243.
Zhuang, L., An, Z., Guo, Y., Zhang, K., Chen, X., Zhang, D., Xue, Z., Zhou, X., Lu, X., 2016. Talanta 161, 713–720.
Zou, M., Li, D., Yuan, R., Xiang, Y., 2017. Biosens. Bioelectron. 92, 624–629.